ChemEurJ

Research Article
doi.org/10.1002/chem.202501914

Chemistry Europe
European Chemical Societies Publishing

www.chemeurj.org

Fluorinated Guanidino-Polyamine Conjugates With Ribonuclease Activity – Toward a Therapeutic Tool for Multi-Drug Therapy

Carola Romani,[a] Paola Gagni,[b] Riccardo Salvio,*[c] Mattia Sponchioni,*[a] and Alessandro Volonterio*[a]

The development of multifunctional carriers for gene delivery is a critical challenge in modern therapeutics, particularly in the context of multi-drug therapy (MDT). In this study, we report the synthesis and characterization of fluorinated guanidino-polyamine conjugates based on low-generation polyamidoamine (PAMAM) dendrimers and low molecular weight polyethyleneimine (PEI) polymers. These conjugates are designed to act as both efficient transfection agents and artificial ribonucleases, providing a dual-function approach to gene therapy. The functionalization with fluorinated guanidino groups enhances DNA condensation, facilitates intracellular delivery, and enables tracking via ^{19}F MRI. Potentiometric and kinetic studies demonstrate their phosphodiesterase activity on a model compound, with PAMAM G4 derivatives exhibiting the highest catalytic efficiency. Biolayer interferometry and transfection experiments confirm mRNA cleavage activity, leading to reduced gene expression. Additionally, transfection studies with plasmid DNA (pDNA) indicate high gene delivery efficiency, surpassing conventional PEI-based systems while maintaining low cytotoxicity. These findings suggest that the conjugates presented herein, and in particular those derived from low-generation PAMAM dendrimers, can serve as promising multifunctional carriers for a combined diagnostic and MDT, offering a new strategy for synergistic gene delivery and RNA degradation.

1. Introduction

"Is it time for multi-drug therapy (MDT) with a combination of therapeutic nucleic acids (TNAs)?"[1] This is the title of a very interesting perspective by Prof. Leśnikowski published early this year on the potential of using therapeutic nucleic acids in an MDT format, an approach that is often adopted successfully with traditional chemoterapeutics.[2–4] Actually, the last decades have witnessed a growing interest toward the use of TNAs to address the prevention and treatment of many diseases that are difficult to tackle with small molecule drugs.[5–7] TNAs can be broadly categorized in three main classes: 1) DNA enabling the replacement, supplementation, or modification of defective genes to induce the production of therapeutic proteins; 2) various forms of RNA, which allow for transient gene expression, gene silencing, or post-transcriptional regulation, providing precise control over cellular processes; and 3) antisense oligonucleotides (AONs), which are short, synthetic single-stranded nucleotides designed to bind to specific mRNA sequences, leading to degradation, splicing modification, or translation inhibition, thus offering a targeted approach for genetic and neurological disorders. Regardless of the specific form of the active molecule, when a systemic administration is required, the development of an efficient delivery system, typically modified viruses or, alternatively, cationic lipidic molecules and polymers, is essential to ensure stability, cellular uptake, and effective action of the TNAs.[8–11] In this context, polyamidoamine dendrimers (PAMAM) and linear or branched polyethyleneimine polymers (lPEI or bPEI, respectively) are the most investigated cationic polymers. This is due to their ability to complex and protect the TNA in the extracellular milieu, thereby improving their internalization efficiency mainly due to electrostatic interactions with the negatively charged cell surface, and their ability to release TNA to the target organelle inside the cell.[12–14] In this direction, low molecular weight (MW) polymers require less sophisticated synthesis and purification processes, allowing a compression in the manufacturing costs, but are notoriously characterized by scarce transfection efficiency (TE). This can be improved through high MW polymers, which unfortunately are associated with high cytotoxicity. To combine the advantages of the two categories while mitigating the corresponding drawbacks, there is a great deal of research in finding suitable functionalization of low MW PAMAM

[a] C. Romani, M. Sponchioni, A. Volonterio
Department of Chemistry, Materials and Chemical Engineering "Giulio Natta", Politecnico di Milano, via Mancinelli 7, Milano 20131, Italy
E-mail: mattia.sponchioni@polimi.it
alessandro.volonterio@polimi.it

[b] P. Gagni
Consiglio Nazionale delle Ricerche, Istituto di Scienze e Tecnologie Chimiche "Giulio Natta" (SCITEC), Via Mario Bianco 9, Milan 20131, Italy

[c] R. Salvio
Dipartimento di Scienze e Tecnologie Chimiche, Università "Tor Vergata", Via della Ricerca Scientifica, 1, Roma 00133, Italy
E-mail: riccardo.salvio@uniroma2.it

Supporting information for this article is available on the WWW under https://doi.org/10.1002/chem.202501914

dendrimers and PEI polymers to increase their ability to transfect cells and possibly to give the carrier multifunctional properties. For instance, the functionalization with linkers containing fluorinated groups may result in better transfecting performance along with the possibility for the polymer to be trackable as an alternative contrast agent in ^{19}F magnetic resonance imaging (MRI) applications.[15,16]

Besides the type of the carrier, TNAs are currently administered as monotherapies.[17] However, just because a carrier is needed, liposomes and/or cationic polymers could be exploited to encapsulate and deliver simultaneously more than one TNAs, as already demonstrated in a few cases to access MDTs.[1,18] Even so, unlike the case of small-molecule MDTs, the clinical application of TNA combinations is still in its infancy. Among the several limitations that render the development of combined TNA therapies difficult, the differences in the electronic and physical properties of the single TNAs are some of the most limiting. One possible solution to overcome this problem could be the design of nanocarriers made by self-assembled biologically active TNAs.[19] Herein, we propose for the first time an alternative solution to overcome this problem by investigating the application of a "conventional carrier," that is, a cationic polymer, having such phosphodiesterase activity, thus acting as an artificial AON, being able at the same time to complex pDNA and efficiently transfect cells.

Recently, we have shown that low generation PAMAM dendrimers functionalized with linkers containing trifluoromethyl moieties along with a guanidino functional group are able to transfect cells very efficiently, being much more performant and less cytotoxic than bPEI 25 kDa, which is considered the gold standard for these applications.[20,21] In this strategy, the presence of the trifluoromethyl group is important for three reasons: 1) it facilitates the "click" functionalization of the polymer, 2) it acts synergistically with the guanidino moiety, improving DNA condensation and intracellular delivery and lowering cellular toxicity, and 3) it renders the conjugates trackable through ^{19}F MRI due to the intense and sharp signals. Moreover, by using a linear linker, we could fine-tune the degree of functionalization by simply playing with the number of equivalents used in the "click" decoration of the outer amino groups of PAMAM dendrimers.[21] Actually, we were able to achieve either full or partial functionalization, providing conjugates still possessing a programmed number of free primary amines on the periphery of the dendrimers, being the latter being more efficient in terms of transfection.[21] This opens up a promising feature, as it has been recently proved that systems having guanidino functional groups along with free primary or secondary amines can have metal-ions-independent RNA-cleaving activity.[22–24] In this direction, the topological structure of dendrimers offers a unique chance to build artificial enzymes.[25] By leveraging this finding here, we report for the first time the preparation and the study of the TE and the catalytic activity as phosphodiesterase of fluorinated macromolecular species, based on low-generation PAMAM G2 and G4 dendritic structures or low MW lPEI and bPEI. This approach is framed within the context of antisense therapy. We believe that a transfecting agent with complementary catalytic activity could have a strong impact on MDT applications. In particular, our agent can act as a catalyst in the cleavage of phosphodiester bonds in ribonucleotides, as extensively demonstrated through potentiometric studies, kinetic analyses using a small-molecule model, and biolayer interferometry. We have also observed mRNA silencing in vitro. Moreover, the agent can complex and deliver pDNA into cells while maintaining its reactivity. This study is then expected to provide a sort of "rule of thumb" and inspiration in designing multifunctional TNA carriers acting as artificial AON.

2. Results and Discussion

2.1. Synthesis of Fluorinated Guanidino-Polyamine Conjugates

Since α,β-unsaturated carbon-carbon double bonds bearing fluorinated moieties exhibit a remarkable reactivity toward nucleophiles due to the presence of the strong electron-withdrawing fluorine atoms,[26–28] we designed linear N′,N″-Boc-protected-N-(6-hexylguanidino)-2-(trifluoromethyl)acrylamide **6** (Scheme 1) as a building block to install trifluoromethyl and guanidine moieties into polymers bearing primary or secondary amines, such as PAMAM G2 and G4 or lPEI 2 kDa and bPEI 600 Da. The Michael addition is straightforward, leading to the clean formation of the corresponding conjugates without the need for heating or any kind of catalysts; that is, click reaction (Scheme 1). As already demonstrated for the PAMAM dendrimers, by controlling the equivalents of the fluorinated building block **6** used in the click functionalization, it was possible to fine-tune the functionalization degree (FD), obtaining after removal of the Boc-guanidino protecting groups conjugates **1**@PAMAM-G2, **2**@PAMAM-G4, **3**@lPEI, and **4**@bPEI, provided with both trifluoromethyl and guanidine moieties along with free primary and/or secondary amines. In addition, the fully functionalized dendrimer **5**@PAMAM-G4 was synthesized to serve as a point of comparison in the measurements described later.

The functionalization of lPEI 2 kDa and bPEI 600 Da was performed in the same reaction conditions used for the grafting of PAMAM dendrimers, that is, methanol as solvent at room temperature, using as many equivalents of building block **6** as the number of secondary amines in lPEI 2 kDa and primary amines in bPEI 600 Da, yielding 65.9% and 66.67% FDs, respectively. The FDs of fluorinated PEI conjugates **3**@lPEI and **4**@bPEI were determined by ^{1}H NMR by integrating characteristic signals belonging to the PEI polymers, that is, the hydrogens of the N-methylene groups, versus the signals belonging to the decorating arm, in particular the hydrogens of the four internal methylene groups of the aliphatic chain resonating at a higher field, according to a well-established procedure (Figure 1A and Table 1).[20,21]

As highlighted in Figure 1B-E, all the conjugates possess a narrow and intense fluorine signal, with the signals of **1**@PAMAM G2, **2**@PAMAM G4, and **4**@bPEI being the sharpest and most intense. This observation is quite surprising, taking into consideration that the polymers are not fully decorated and that the click reaction generates a stereogenic center leading to the formation of a mixture of diastereoisomers. However, the presence of a single, sharp signal suggests that the trifluoromethyl

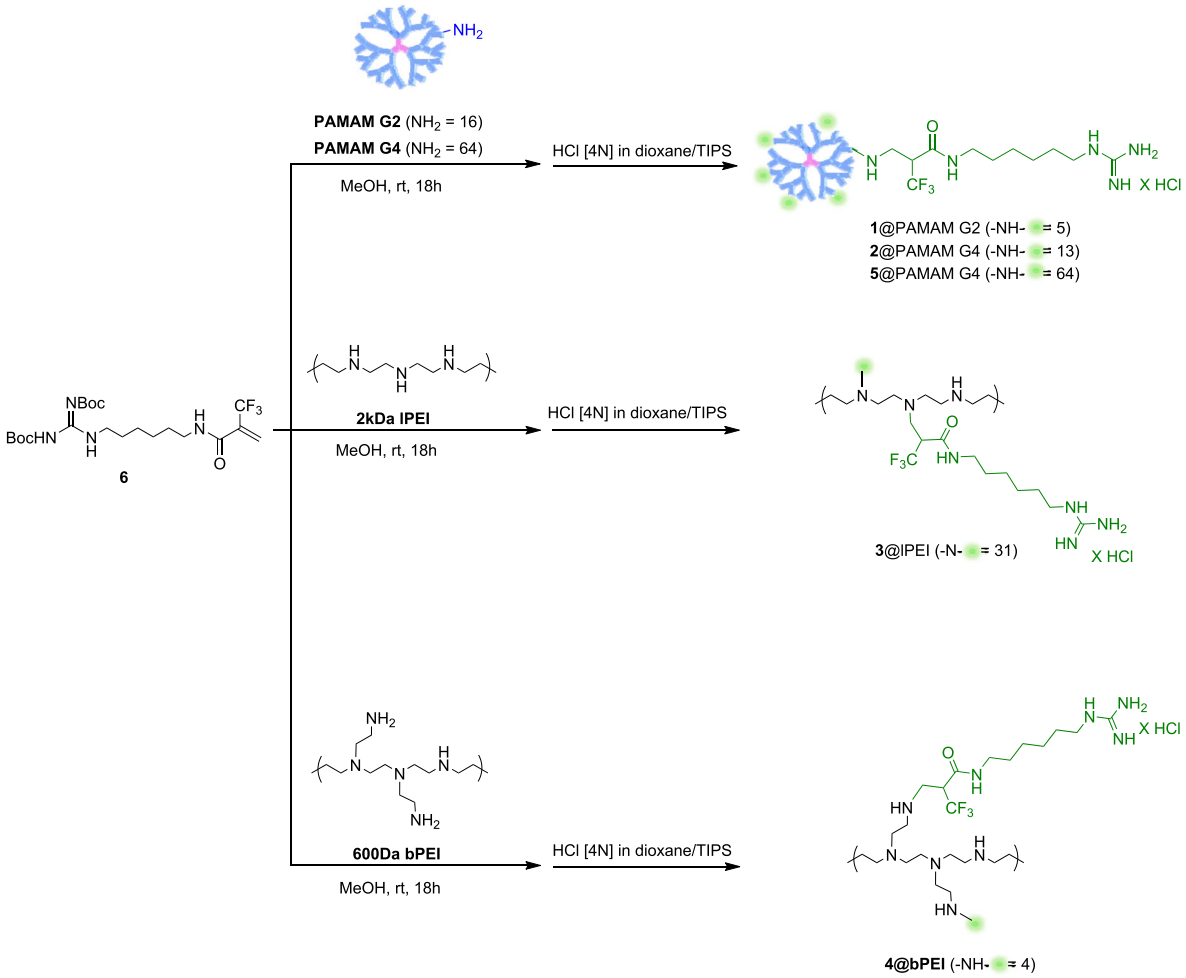

Scheme 1. Synthesis of guanidino-fluorinated PAMAM and PEI conjugates **1**–**5**.

groups are quite flexible within the tridimensional structure of the conjugates resulting to be magnetically equivalents. These characteristics make conjugates **1**–**4** ideal candidates for a possible implementation as ^{19}F MRI contrast agents.

2.2. Potentiometric titrations

The investigation of the acid–base properties of the functionalized polymers is an important prerequisite for a rigorous study of their activity as phosphodiesterases. The compounds were titrated with a standard solution of tetramethylammonium hydroxide in water in the presence of 10 mM tetramethylammonium perchlorate as an ionic strength buffer. The titration plots for **1**@PAMAM G2 and **2**@PAMAM G4 (Figure 2A, red and blue plots, respectively) and the elaboration of the experimental data indicate the presence of a number of titratable protons in the pKa range of 7.3–8.5. The slightly higher acidity of the amines can be ascribed to the electrostatic repulsion exerted by the extremely high positive charge density generated by the other guanidinium and ammonium groups. After the titration of the ammonium functions, the pH steeply rises upon the addition of further amounts of titrating solution as an indication of the complete deprotonation of all the amines. The pH step relative to the deprotonation of guanidinium units is not visible, probably because of the high intrinsic pKa value of this unit, that is, 13.7,[29] that overlaps with the acidity of the solvent water molecules. The same titration experiments were also performed on polymers **3**@lPEI and **4**@bPEI (Figure 2, magenta and black plots, respectively). Their potentiometric behavior closely resembles that of dendrimers, with apparent pKa values around 8.0. This deprotonation is attributed to the ammonium groups present in the polymer.

These experiments provide the number of titratable protons on a single dendrimer/polymer molecule, confirming the values determined by ^{1}H NMR spectra as shown in Table 2. In the same Table 2, the overall number of functions and the ratio between the number of guanidinium units and amines are reported as well.

2.3. Kinetic measurements of the phosphodiesterase activity on an RNA model compound

In a preliminary series of experiments, the phosphodiesterase activity of the synthesized compounds has been evaluated using 2-hydroxypropyl *p*-nitrophenyl phosphate (HPNP, Scheme 2). This

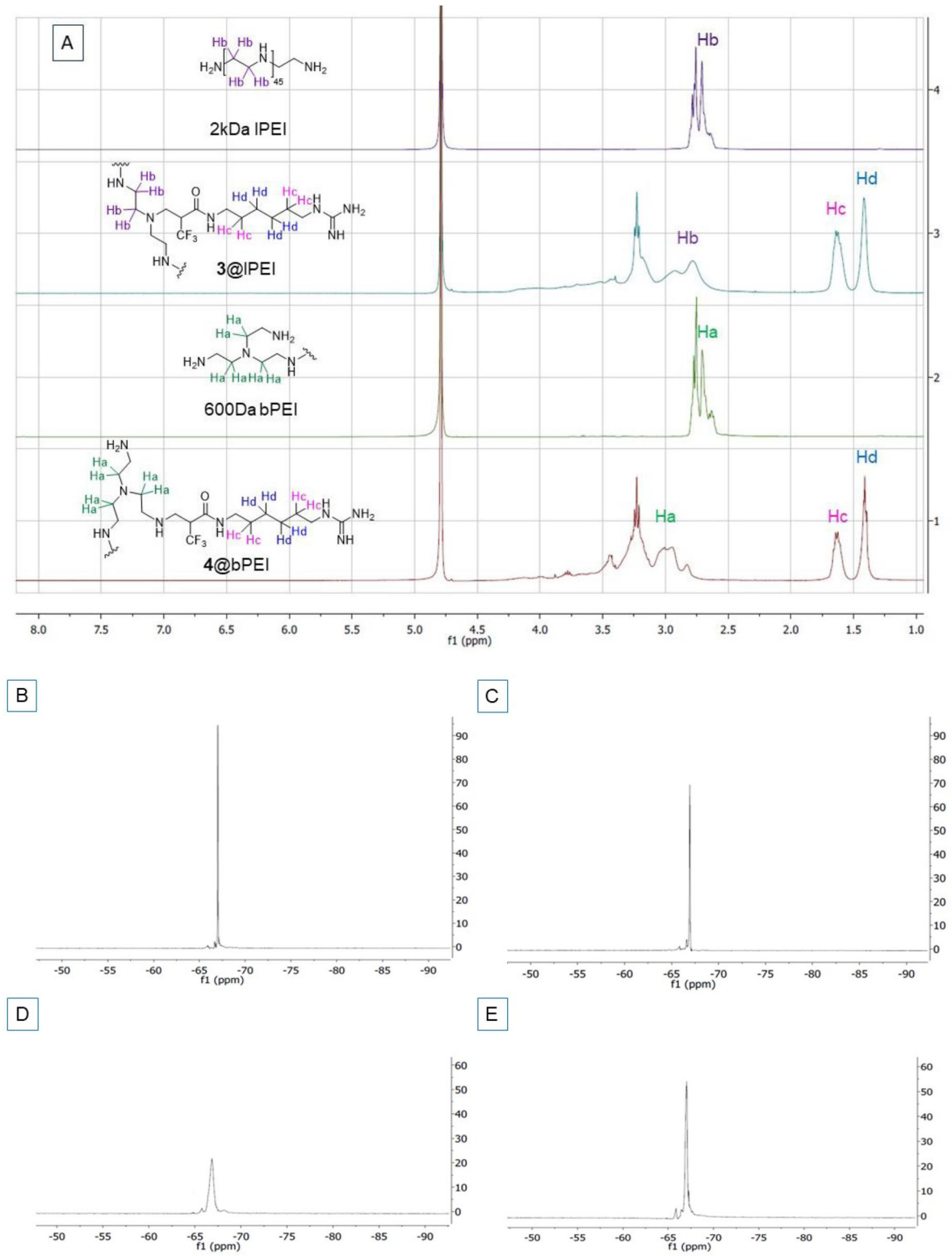

Figure 1. In Figure A the ^{1}H NMR spectra recorded in D_2O of 2 kDa lPEI (violet spectrum), **3**@lPEI (light blue spectrum), 600 Da bPEI (green spectrum), and **4**@bPEI (red spectrum) are reported. The fluorine signals of **1**@PAMAM-G2 (Figure 1B), 2@PAMAM-G4 (Figure 1C), **3**@lPEI (Figure 1D), and **4**@bPEI (Figure 1E) are reported in Figure B-E.

Table 1. Chemical characterization of fluorinated PEI guanidino conjugates **3–4**.

^{1}H relative integrations

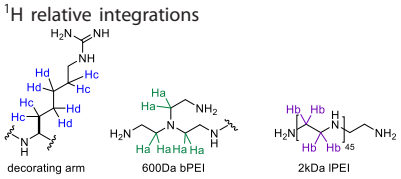

Compound	Hc, Hd	Ha	Hb	Hydrogens belonging to lPEI	Hydrogens belonging to bPEI	# of guanidine grafted (FD %)	Calculated MW [g/mol]	δ [ppm] ^{19}F-NMR
3@lPEI	122.64	180	-	180	-	31 (65.9)	10 422	−66.85
4@ bPEI	16.11	–	24	–	24	4 (66.7)	1832	−66.97

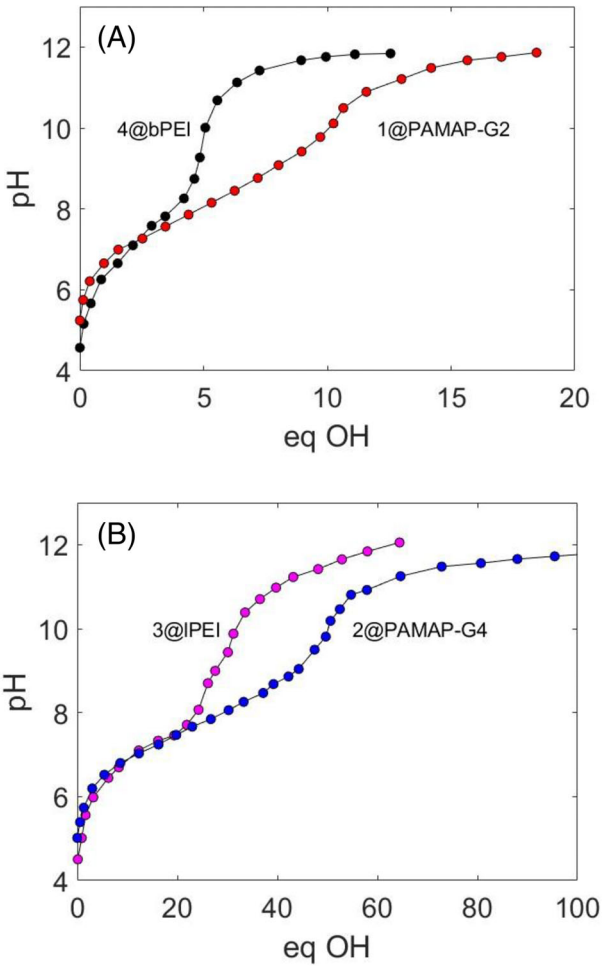

Figure 2. Potentiometric titration plots of a 0.30 mM solution of **1**@PAMAM G2 (red, Figure 2A), **2**@PAMAM G4 (blue, Figure 2B), **3**@lPEI (magenta, Figure 2B), and **4**@bPEI (black, Figure 2A) with Me_4NOH in water (10 mM Me_4NClO_4 at 25 °C), pH value versus OH equivalents.

phosphodiester can be considered as an RNA model compound, as it features a hydroxy group on the 2-position on the propyl chain able to perform an intramolecular nucleophilic attack onto the phosphorous atom, mimicking the hydroxyl in 2′ position on the ribose rings of RNA strands.[30] The reaction generates a 5-membered cyclic phosphate and liberates an equivalent of *p*-nitrophenol, whose concentration can be detected by UV-Vis spectrophotometry. The measurements were carried out in water at 25 °C at different concentrations of **1–5**. Since the number of units on each compound significantly differs, as highlighted in Table 2, the compounds were tested at the same active unit concentration, that is, 0.5 mM, in order to allow a meaningful and rigorous comparison among their activities.

The pH may also be a crucial parameter to control in order to obtain a detectable catalytic activity. In previous studies we had indications that the cleavage of this substrate may occur due to the cooperation of two active functions,[31] one of them involved in the activation and the other acting as a base. On the basis of the potentiometric experiments described above, we carried out the measurements with the water solution buffered at pH 8.0. This condition is a good compromise, as it guarantees that a significant number of amines are in their deprotonated form. On the other hand, it also minimizes the rate of the spontaneous cleavage that increases at high pH values, reducing the acceleration over the background reactivity.

The pseudo-first-order rate constants for the HPNP transesterification reaction in the presence of additives **1**@PAMAM G2, **2**@PAMAM G4, **3**@lPEI, and **4**@bPEI are reported in Table 3 (entries 1–4), together with the dimensionless acceleration ratio over the background reaction (k_{obs} / k_{bkg}). In entries 5 and 6 (Table 3), the activity of the fully guanidinylated (95%) dendrimer **5**@PAMAM G4 and undecorated bPEI 25 kDa, respectively, were reported as negative control.

All the compounds turned out to catalyze the transesterification of HPNP but with different efficiencies. The PEI polymers **3**@lPEI and **4**@bPEI show a catalytic activity advantage of around 80–90 fold over the spontaneous transesterification reaction (Table 3, entries 3 and 4, respectively). The second-generation fluoridated dendrimer **1**@PAMAM G2 exhibits a catalytic activity as high as 290-fold over the k_{bkg} value, definitely higher than the branched or linear polymeric counterparts. However, the best catalytic performance is reached in the presence of the 4th generation dendrimer **2**@PAMAM G4, which overcomes by three orders of magnitude the spontaneous reactivity of the phosphodiester (Table 3, entry 2). On the other side, as expected, fully decorated polymer **5**@PAMAM G4 and undecorated bPEI 25 kDa exhibit poor catalytic activity (entry 5 and 6, respectively),

Table 2. Active functions present on the investigated dendrimers/polymers.

Compound	Formula weight [Da]	Overall number of functions per molecule[a]	Number of free amines per molecule[b]	guanidinium/overall number of functions ratio[c]
1@PAMAM G2	4650	16	11	0.31
2@PAMAM G4	17842	64	51	0.20
3@lPEI	10422	47	16	0.66
4@bPEI	1832	6	2	0.67
5@PAMAM G4	30567	64	3[d]	0.95

[a] determined from the molecular weight and the nature of the dendrimer/polymer.
[b] average number of free amines per molecule determined from the titration experiment and ^{1}H NMR integration.
[c] ratio between the number of guanidinium units and the overall number of functions in the dendrimer/polymer.
[d] determined solely through ^{1}H NMR integration.

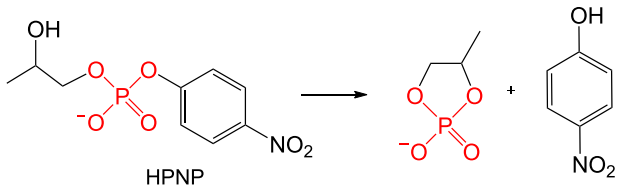

Scheme 2. Model reaction for measuring the phosphodiesterase activity.

Table 3. Transesterification reaction of the RNA model compound HPNP in the presence of the indicated additives in water.[a]

Entry	Additive	Additive concentration [μM][b]	k_{obs} [s^{-1}][c]	k_{obs} / k_{bkg}[d]
1	**1**@PAMAM G2	31.2	6.8×10^{-5}	290
2	**2**@PAMAM G4	7.8	2.6×10^{-4}	1100
3	**3**@lPEI	10.0	2.1×10^{-5}	91
4	**4**@bPEI	83.0	1.9×10^{-5}	82
5	**5**@PAMAM G4	7.8	2.6×10^{-6}	11
6	bPEI 25kDa	2.0	2.3×10^{-6}	10

[a] The k_{obs} values reported were measured via the initial rate method by monitoring the liberation of *p*-nitrophenol. HPNP initial concentration $[HPNP]_i = 0.2$ mM, T = 25.0 °C, 10.0 mM of tetramethylammonium perchlorate. pH 8.0 (phosphate buffer).
[b] The concentrations of the polymer/dendrimer has been chosen in order to guarantee the same molar concentration of active functions, that is, 0.50 mM.
[c] The k_{obs} values were calculated as follows: v_o / $[HPNP]_{Initial}$; estimated error limit = ± 8%.
[d] k_{bkg} at pH 8 = 2.3×10^{-7} s^{-1}, obtained in the kinetic data reported in references 23, 24.

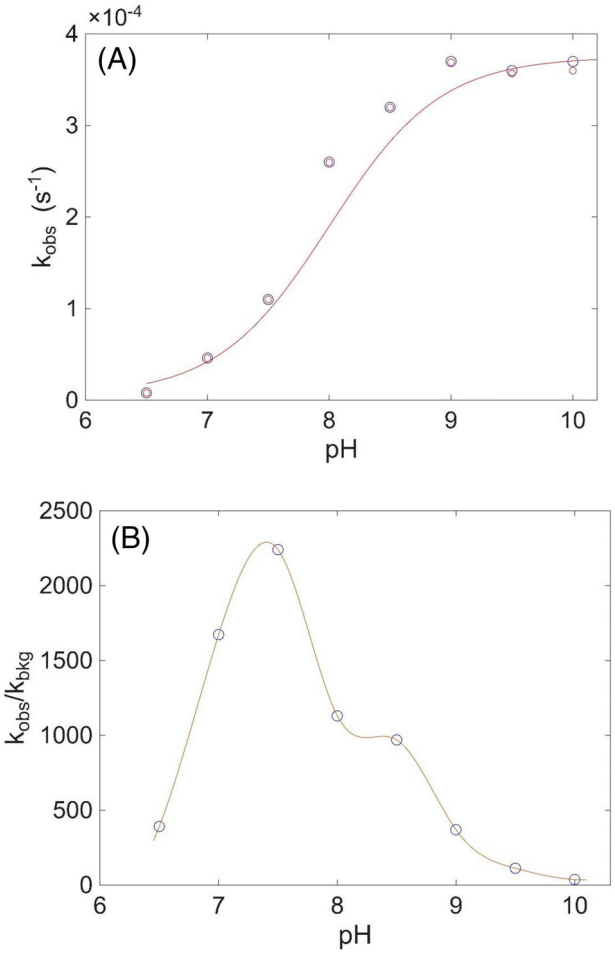

Figure 3. HPNP transesterification catalyzed by **2**@PAMAM G4 at different pH values. (A) k_{obs} rate constants versus pH value; the red dots represent the k_{obs} values corrected for the background uncatalyzed reaction. (B) acceleration over the spontaneous cleavage at different pH values.

lacking free primary amines or guanidino groups, respectively. This evidence highlights the importance of both functions, that is, amines and guanidino groups, in the catalytic mechanism. Interestingly, very similar results were achieved by performing the experiments in the presence of 50% of serum, suggesting a possible reliable activity also in vivo (see Table S1 in Supporting Information).

Since the protonation state of the active functions may play an important role in the catalytic process, in another set of kinetic experiments, the catalytic activity of the most active system, **2**@PAMAM G4, was measured in a wider range of pH values. Pseudo-first-order rate constants for the transesterification of the same substrate, also corrected for the background contributions, are reported in Figure 3 (see also Table S1 in Supporting Information). The spontaneous cleavage remains negligible in the considered pH interval.

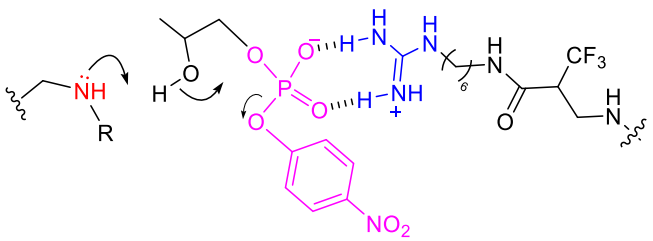

Figure 4. Postulated bifunctional catalytic mechanism for the cleavage of the RNA model by **2**@PAMAM G4 and the other materials involving the cooperative action of an amine acting as a general base and a guanidinium unit behaving as an electrophilic activator.

The transesterification rate of the RNA model increases upon a pH increase. A maximum of activity is reached around pH 9.0, and no further rate increment is observed at higher pH. This experimental picture points to the existence of a bifunctional catalysis that arises from the combined action of a deprotonated amine, acting as a general base, and a protonated guanidine, acting as a general acid/electrophilic activator, as schematically depicted in Figure 4. Most likely the catalytic activity does not rise further over pH 9 because of the complete deprotonation of all the amine functionalities. Interestingly, the catalytic activity of amines/ammonium, in comparison with that of the guanidine/guanidinium or amine/guanidinium dyad, has been proved to be negligible in numerous previous studies.[22,30,32,33] This is probably ascribable to an optimal activity around neutrality and/or an intrinsic activation capability of the guanidinium unit.[22,30]

Figure 3b (see also Table S2 in Supporting Information) reports the acceleration factor versus the pH. The plot indicates a maximum advantage over the spontaneous cleavage around pH 7.0–7.5, particularly advantageous for the biological exploitation of this mechanism in a biological system. At pH 8.0 the advantage is lower but still exceeds three orders of magnitude the spontaneous cleavage. A significant decrease is observed at pH over 9, as the base-catalyzed spontaneous transesterification rate rises significantly in alkaline conditions.

A plot of initial rate versus substrate concentration for the **2**@PAMAM G4 catalyzed transesterification of HPNP shows a linear trend only at low substrate concentration (Figure 5). However, at higher HPNP concentration, a significant deviation from the linearity is observed. This downward curvature is typical of saturation kinetics in which a fast pre-equilibrium with the catalyst precedes the substrate conversion, Equation 1. The reaction rate versus the substrate concentration is given by Equation 2. The nonlinear least-squares fitting of the experimental data to this equation affords the following values of the adjustable parameter: $K_b = (540 \pm 90)\ M^{-1}$, $k_{cat} = (6.2 \pm 1.1) \times 10^{-3}\ s^{-1}$. Because of the low value of binding constant, at the concentration of the kinetic experiments, that is, 0.2 mM substrate concentration, the catalyst works under subsaturating conditions, as less than 10% of the catalyst is bound to HPNP.

$$\mathbf{2}@PAMAM\text{-}G4 + HPNP \underset{\leftrightarrow}{\overset{K_b}{}} \mathbf{2}@PAMAM\text{-}G4 \cdot HPNP \overset{k_{cat}}{\rightarrow} P + \mathbf{2}PAMAM\text{-}G4 \quad (1)$$

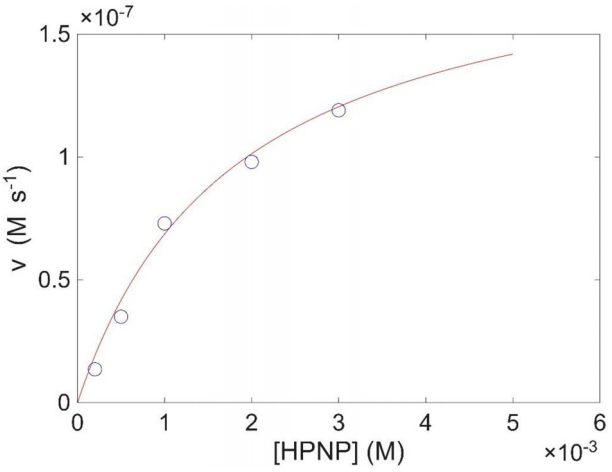

Figure 5. Initial rate of *p*NPhOH liberation versus substrate concentration for the HPNP transesterification carried out in the presence of **2**@PAMAM G4 in water (pH 8.0, 25.0 °C). The points are experimental data, and the curve is least-squares fitting to this data of Equation 2 with the best-fit values of K_b and k_{cat} reported in the text.

$$v = \frac{d[pNPhPH]}{dt} = \frac{K_b k_{cat} C_T [HPNP]}{1 + [HPNP] K_b} \quad (2)$$

2.4. Ribonuclease activity evaluation by bio-layer interferometry

Biolayer interferometry (BLI) is an optical biosensor technique for real-time, label-free analysis of biomolecular interactions.[34] It is useful for kinetic analyses, analyte detection, and quantitation with mid-to-high throughput. BLI has supported various activities in drug design and development, including screening of fragment and compound libraries, analyzing structure-activity relationships, and selectivity of small-molecule drug leads, but to our knowledge it has never been used either to characterize gene delivery vectors or to evaluate RNA cleavage catalytic activities. The ribonuclease activity of **2**@PAMAM G4, which was demonstrated to be particularly efficient in the preliminary experiments, was observed for the first time by BLI on mRNA sequences. As streptavidin (SA) biosensors were used, **2**@PAMAM G4 polymer was biotinylated to allow biosensor loading prior to evaluating the binding with mRNA. Initially, **2**@PAMAM G4 was conjugated with commercially available NHS-PEG_4-Biotin with different molar ratios: one biotin per free amine (protocol A) or one biotin per polymer (protocol B). A non-biotinylated **2**@PAMAM G4 was preserved as a negative control. As reported in Supporting Information (Figure S2), both biotinylating protocols worked properly (blue and red lines, respectively), while very low nonspecific binding was measured on the negative control (green line).

Subsequently, 25μg/mL of mRNAfluc was used to evaluate the binding of a generic RNA on biosensors loaded with polymers. We observed that protocol B is the best strategy for **2**@PAMAM G4 biotinylation while preserving its ability to still interact with nucleic acids (Figure S3 and Table S3 in Supporting Information).

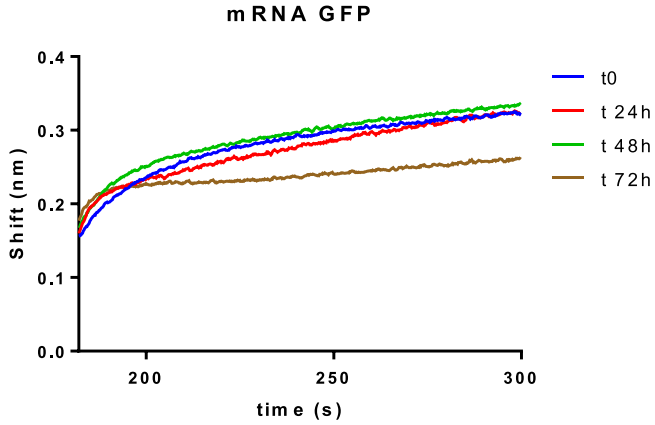

Figure 6. BLI measurements of the association step between 25μg/mL mRNAfluc and **2**@PAMAM G4-biotin loaded on streptavidin tips.

Stated the higher performances of one biotin per polymer, incubations were repeated under the same protocol set-up on the mRNAgfp used for the in vitro transfection assays (see below) in order to monitor its stability in RNAse-free PBS at 37 °C up to 72 hours (Figure 6), sampling at 0, 24, 48, and 72 hours, by comparing the binding on **2**@PAMAM G4 and undecorated PAMAM G4, both bearing biotins. We observed that mRNAgfp was stable for the first 48 hours, then lower binding capabilities on biotinylated **2**@PAMAM G4 were measured. A global analysis of the first three curves (time 0, 24, and 48 hours) provided an average association value (Ka) equal to 9.306E + 03 1/Ms when using **2**@PAMAM G4-biotin and 1.631E + 04 1/Ms when using commercial PAMAM G4-biotin on the biosensor, revealing a stronger interaction for **2**@PAMAM G4-biotin for the substrate.

Following these results, we incubated 25μg/mL mRNAgfp with **2**@PAMAM G4 or PAMAM G4, respectively, and monitored the stability at 37 °C, over time, sampling at 0, 24, and 48 hours, by comparing the binding on **2**@PAMAM G4-biotin and undecorated PAMAM G4-biotin, respectively. The complex with the undecorated dendrimer remains stable up to 48 hours (Figure 7A), while significant changes in bindings happen when incubating mRNAgfp with **2**@PAMAM G4 (Figure 7B) with a progressive decrease in both plateau level and association value (Ka).

Ka values (Table S4 in Supporting Information) decrease exponentially for both complexes, providing the highest differences between the two polymers within the first 24 hours (Figure 8); no significant changes happen between 48 and 72 hours.

The instrument recorded both association and dissociation steps to eventually provide avidity estimation of the complexes as the ratio between dissociation and association values. However, due to the complexity of the interaction between the dendrimer and the nucleic acid and its consequent bifunctional catalysis, association and dissociation steps have been studied separately. Indeed, the behavior of the two biotinylated polymers, **2**@PAMAM G4 and PAMAM G4, differs even more when considering the dissociation phase (Figure 9). No dissociation value (Kd) could be measured on **2**@PAMAM G4, as barely any dissociation was observed, mainly due to the small pieces of nucleic acids still in dynamic equilibrium during this phase. This complex behavior of our systems can be explained as addressed to multivalent and dynamic interactions. On the contrary, PAMAM G4, which does not have the catalytic effect to generate a complex mixture of nucleic acid fragments, provides stable interactions within 48 hours, thus allowing the measurement of global kinetic parameters in terms of Ka 7.383E + 05 1/Ms and Kd 2.73E-04 1/s.

Although the multivalent interaction between **2**@PAMAM G4 and mRNAs, we have been able to demonstrate the stability of the mRNAgfp up to 48 hours in experimental conditions (25μg/mL in RNase free PBS, 37 °C). Furthermore, these results corroborate the ribonuclease catalytic activity of our dendrimer on nucleic acids, with a peak of activity within the first 24 hours. Of notes, to our knowledge, this is the first time ever applying BLI on a gene delivery vector characterization as well as on measuring any nucleic acids catalytic activity.

2.5. Biophysical characterization, in vitro cytotoxicity and transfection of 3@lPEI and 4@bPEI conjugates

With the aim of exploiting decorated polymers **1**–**4** in MDT, combining their phosphodiesterase activity with the delivery of pDNA,[16] we investigated their biophysical properties, TE, and cytotoxicity on human umbilical vein endothelial cells (HUVECs) and compared them to those of the gold standard in this field, bPEI 25 kDa. As shown in Figure S4 (Supporting Information), agarose gel analysis revealed that all the decorated polymers efficiently complex the gene cargo (pGFP) at an N/P ratio as low as 5. This is an interesting feature for PEI derivatives having low molecular weights that generally require a high value of N/P ratio to be able to fully condense the genetic materials.[35] However, while the hydrodynamic diameter (DH) of the polyplex formed by mixing **3**@lPEI with pDNA at N/P 15, like those with **1**@PAMAM G2 and **2**@PAMAM G4, was in the range of 200 nm, thus suitable for gene transfection,[36] the corresponding polyplex formed with **4**@bPEI resulted to be twice bigger (Table S5, Supporting Information). This is probably the reason for the inefficiency of **4**@bPEI in transfecting cells (see below).

The results of TEs and cytotoxicity of the investigated conjugated polymers are shown in Figure 10.

All the cationic polymer vectors reported in this work demonstrated very poor cytotoxicity when administered to HUVECs (Figure 10C). Indeed, the cell viability for these candidates was invariably larger than 85% and decisively higher than the standard cationic polymer bPEI 25 kDa. From the analysis of the TE (Figure 10A, B), it is possible to observe that both **1**@PAMAM G2 and **2**@PAMAM G4 exhibited very promising delivery and release of the genetic cargo to the cells, leading to the expression of GFP. Indeed, the transfected cells for these conjugates were significantly larger than for bPEI 25 kDa. This was overcome in terms of TE also by **3**@lPEI, even though its TE was lower with respect to both **1**@PAMAM G2 and **2**@PAMAM G4. Disappointingly, the TE of conjugate **4**@bPEI was very low, probably due to low MW and the unfavorable biophysical properties. These results, taken together with the

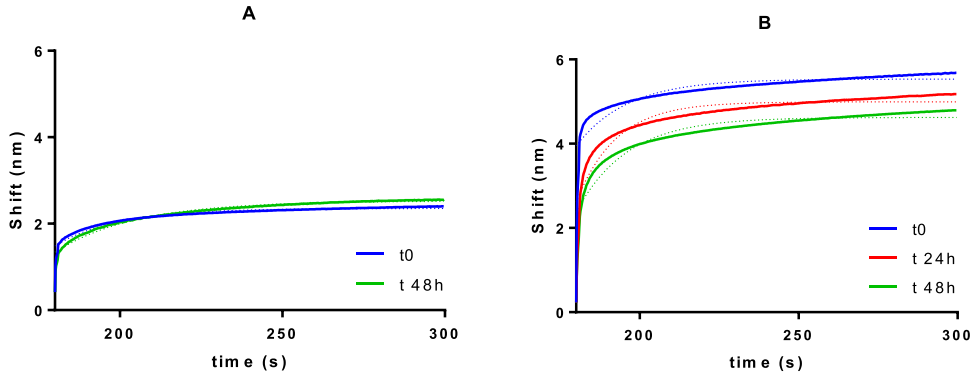

Figure 7. A) BLI measurements of the association step between PAMAM G4-biotin and 25μg/mL mRNAgfp preincubated with PAMAM G4 up to 48 hours (blue line at t0; green line after 48 hours of coincubation). B) BLI measurements of association steps between **2**@PAMAM G4-biotin and 25μg/mL mRNAgfp preincubated with **2**@PAMAM G4 up to 48 hours (blue line at t0; red line after 24 hours of coincubation; green line after 48 hours of coincubation). Dotted lines depict a nonlinear fitting one-phase association curve.

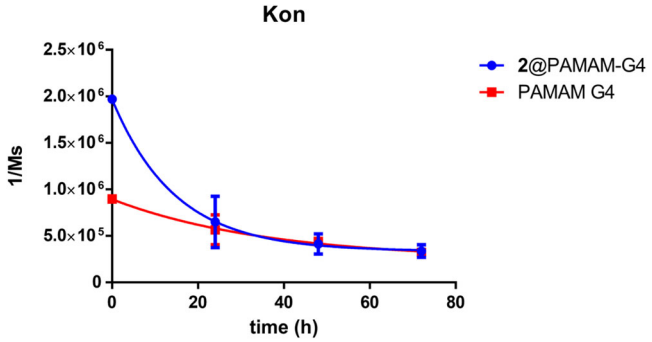

Figure 8. Association rate decay by time. Experimental data interpolated with a *nonlinear regression exponential one-phase decay* curve. Error bars indicate the positive and negative experimental deviations as reported in the data tables S3 and S4 in Supporting Information.

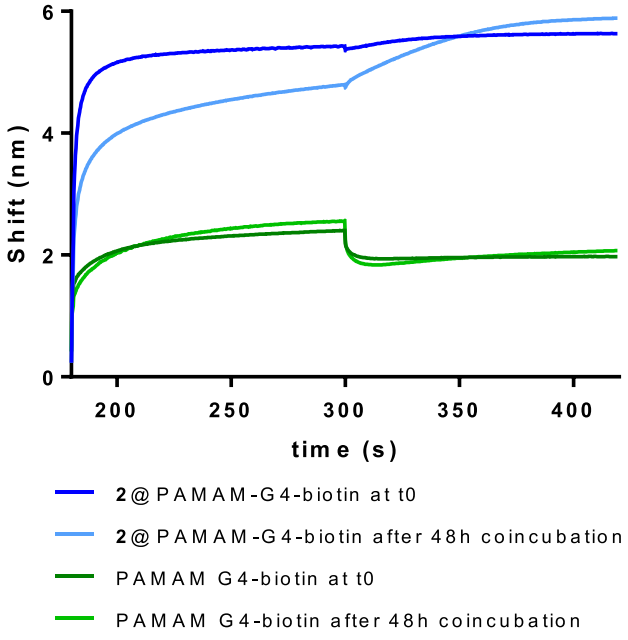

Figure 9. BLI measurements of association and dissociation steps between **2**@PAMAM G4-biotin (blue lines) or PAMAM G4-biotin (green lines) and 25μg/mL mRNAgfp preincubated with either **2**@PAMAM G4 or PAMAM G4, respectively, up to 48 hours.

phosphodiesterase activity of the conjugates **1**–**4** described above, suggest that derivatives **1**@PAMAM G2 and **2**@PAMAM G4 are the best candidates for a possible MDT application.

2.6. In vitro Evaluation of Ribonuclease Activity

To assess the phosphodiesterase activity of **2**@PAMAM G4, which showed the highest efficiency in the exploratory experiments with the model compound HPNP, in an intracellular environment, a preliminary in vitro test was conducted using the HeLa cell line. The cells were transfected via the nonviral vector 25 kDa bPEI with mRNA expressing GFP and then incubated with the PAMAM conjugate. The phosphodiesterase activity was then evaluated by measuring the fluorescence intensity compared to the untreated control group (w/o cat). A decreased fluorescence intensity was considered indicative of mRNA cleavage, which would prevent mRNA-GFP translation in treated cells (w/ cat). The tests were performed using three different catalyst concentrations, designed to cleave 1/10, 1/40, and 1/100 of the total phosphate groups present in mRNA-GFP (Figure 11A-C. For the corresponding transfected cell micrographs acquired with Celena S microscopy (filter cube GFP), see Figure S5 in Supporting Information). These concentrations were based on the molar ratio between the catalyst and HPNP, as described in the previous section, scaled up for mRNA.

25 kDa bPEI, used as a positive control, led to 25% of GFP-positive cells after 48 hours when no catalyst was added to the culture medium. The incubation of the cells with **2**@PAMAM G4, instead, resulted in a significant reduction of GFP-positive cells to 5% (Figure 11A). These results suggest that the catalyst exhibits mRNA cleavage ability within 24 hours of treatment, which is consistent with what we observed when investigating the catalytic activity of **2**@PAMAM G4 through BLI (Figure 8). Notably, the catalyst maintained its effect even at lower concentrations where the number of GFP-positive cells could be reduced to 10% at a stoichiometric ratio of 1/40 and to 20% at 1/100 (Figure 11C). Furthermore, a supplementary investigation was conducted to assess the phosphodiesterase activity of **2**@PAMAM G4 by using the conjugate itself as both an mRNA

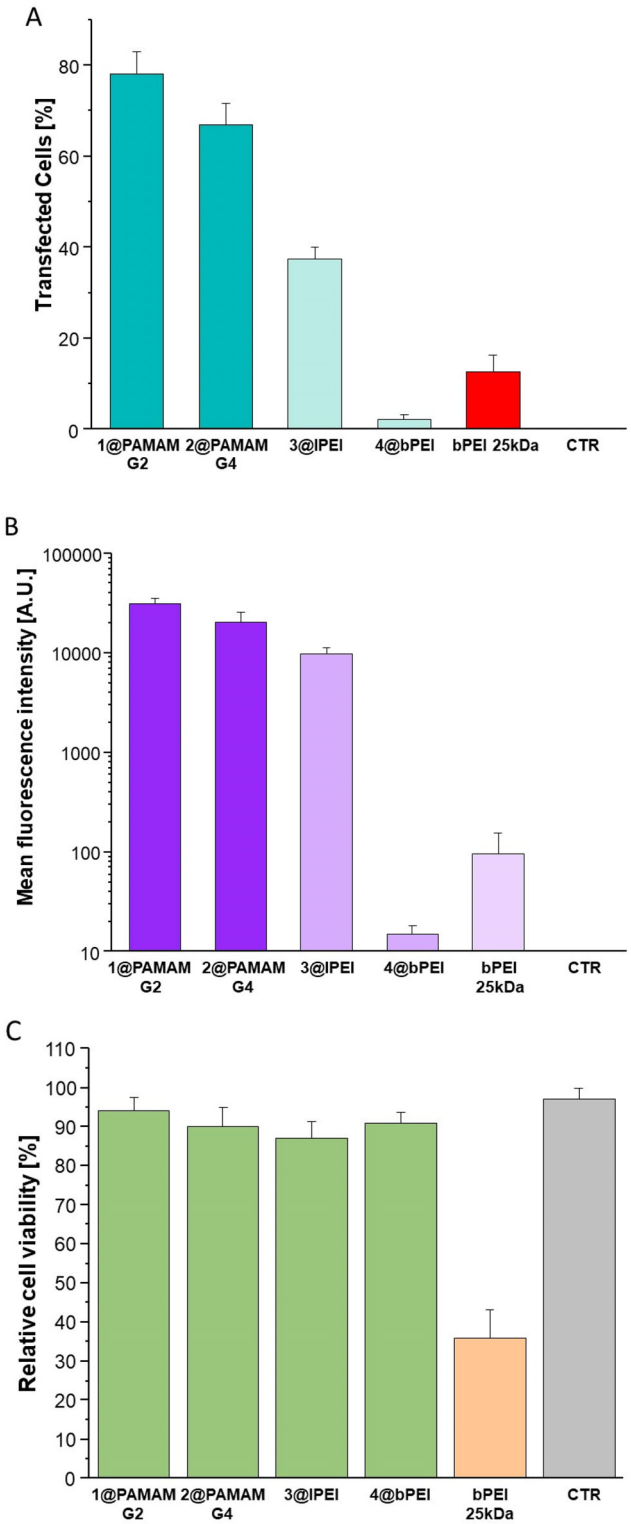

Figure 10. Cytotoxicity and TEs of **3**@lPEI and **4**@bPEI compared to **1**@PAMAM G2, **2**@PAMAM G4, and bPEI 25 kDa (N/P fixed to 15).[21] Figure A and B depict TE tests at N/P 15, as percentage of transfected cells and fluorescence intensity measured via ImageJ software, respectively, after 48 hours. For negative control (CTR), HUVECs without the transfecting agent were considered. Figure C depicts cytotoxicity as cell viability relative to the control; error bars are standard deviation, and statistical significance is $p < 0.0001$ for all polymers compared to positive control bPEI 25 kDa, determined by Student's t-test and considering $p < 0.05$ as significant. All experiments were conducted in quadruplicate ($n = 4$).

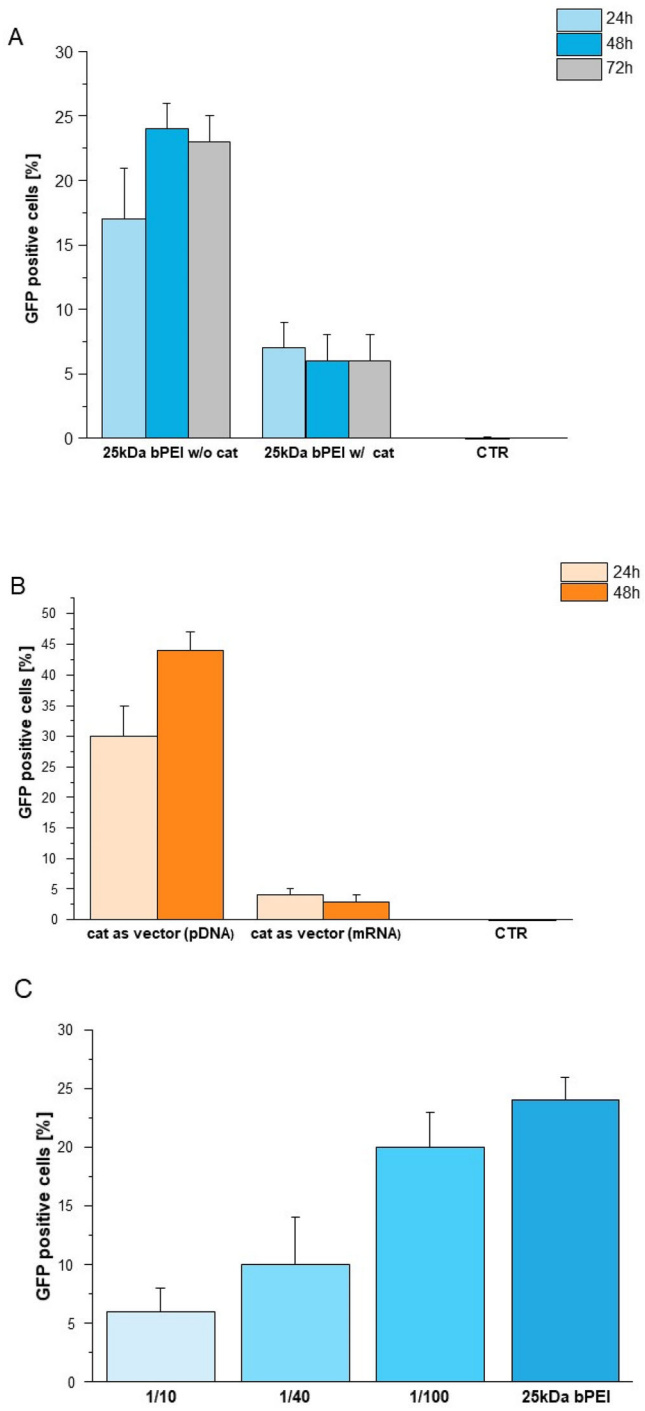

Figure 11. A) GFP-positive cells at different time points after transfection in the presence and absence of the catalyst; B) GFP-positive cells when these are transfected using **2**@PAMAM G4 delivering mRNA or pDNA. The number of positive cells was measured after 24 hours and 48 hours. For negative control (CTR), HeLa without transfecting agent were considered; C) GFP-positive cells when incubated with different concentrations of catalyst and compared with 25 kDa bPEI. Error bars are standard deviation, and statistical significance is $p < 0.001$ compared to bPEI 25 kDa w/o cat, determined by Student's t-test and considering $p < 0.05$ as significant. All experiments were conducted in quadruplicate ($n = 4$).

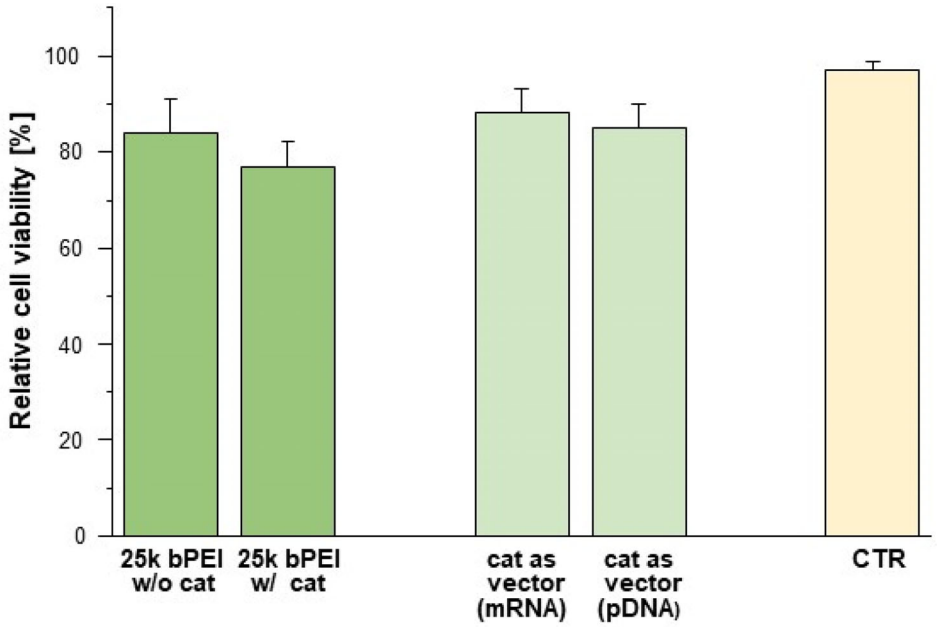

Figure 12. Cytotoxicity of **2**@PAMAM G4 as a gene delivery vector compared to bPEI 25 kDa w/ and w/o **2**@PAMAM G4 expressed as cell viability relative to the control. Error bars are standard deviation (SD), and statistical significance is $p < 0.001$ for all samples compared to untreated cell control (CTR), determined by Student's t-test and considering $p < 0.05$ as significant. All experiments were conducted in quadruplicate ($n = 4$).

and plasmid (pDNA) delivery vector (Figure 11B). When the catalyst was used as an mRNA delivery system, the number of GFP-positive cells remained below 5% and constant over 72 hours from treatment. In contrast, cells treated with pDNA-GFP complexed by **2**@PAMAM G4 exhibited a TE ranging from 30% to nearly 45% within 48 hours. These results suggest that the lower number of GFP-positive cells observed in the mRNA delivery is likely due to the cleavage of the nucleic acid by the catalyst rather than a deficiency in its gene delivery capability.

Finally, to eliminate bias arising from the varying cytotoxicity of the tested delivery vectors/polyplexes, we performed an MTT viability assay in the presence of bPEI 25 kDa with (w/) and without (w/o) the catalyst **2**@PAMAM G4 and of the polyplexes **2**@PAMAM G4 with mRNA and 2@PAMAM G4 with pDNA, which indicated high viability of treated cells (Figure 12 and Figure S6).

3. Conclusions

In an attempt to realize a fully multifunctional medical tool, able to act as gene delivery vector, ^{19}F MRI contrast agent, and a target RNA cleaving agent in the frame of the MDT format, we investigated the preparation and the catalytic activity as phosphodiesterase of fluorinated macromolecular species, based on low generation G2 and G4 PAMAM dendritic structures and low MW linear lPEI and bPEI. The conjugates **1**@PAMAM G2, **2**@PAMAM G4, **3**@lPEI, and **4**@bPEI presented in this study have been prepared starting from the corresponding polyamine polymers by a straightforward reaction with an electrophilic fluorinated building block bearing a guanidino functional group. The reaction conditions of the "click" Michael addition were controlled to obtain partially derivatized materials provided with both guanidino units and free primary or secondary amines. The potentiometric investigation and the kinetic analysis on a model molecule demonstrated the remarkable efficiency of these materials in hydrolyzing the phosphodiester functional group, especially those based on the PAMAM dendrimer, and provided convincing insights about the reaction mechanism. The phosphodiesterase activity of the PAMAM-derived conjugate **2**@PAMAM G4, which showed the best catalytic activity with the small molecule mimic, was also tested in mRNA cleavage via biolayer interferometry with a clear indication of partial ribonucleotide cleavage in a time range of 24–48 hours. It is worth noting that this is the first time that biolayer interferometry was employed for this application, providing a reliable new tool to investigate phosphodiesterase activity of polymers on RNA biomacromolecules. The remarkable catalytic activity of **2**@PAMAM G4 was confirmed in biological experiments on HeLa cells. This vector was able to suppress the signal originated from the translation of an mRNA encoding for GFP. On the other side, when used as a delivery system for pDNA, it maintained high TE and low cytotoxicity. Taking also into consideration that oligonucleotides tethered to the surface of PAMAM dendrimers have been demonstrated to maintain their ability to form hydrogen bond networks with their targets (selectivity),[37] the whole experimental picture points to the possibility of employing the presented dendrimers as multipurpose medical tools in MDT settings, being able to behave both as a diagnostic (^{19}F MRI) and curative device.

4. Experimental Section

Materials: PAMAM G2 and PAMAM G4 dendrimers (ethylenediamine core, 16 and 64 surface groups, respectively), 2 kDa lPEI,

25 kDa and 600 Da bPEI, and all other organic reactants, solvents, and culture reagents were purchased from Sigma-Aldrich (Milan, Italy) if not differently specified and used as received. Use of a cationic polymer based on PEI for transfection is covered by US Patent 6013240, European Patent 0770140, and foreign equivalents, for which Polyplus-transfection is the worldwide exclusive licensee. Linker **6** was synthesized according to the literature (Ref. 20). Spectra/Por dialysis bags (MWCO = 1 and 8 kDa) were from Spectrum Laboratories (Compton, CA, USA). The green fluorescent plasmid (Monster Green Fluorescent Protein phMGFP Vector) encoding for the modified green fluorescent protein was purchased from Promega (Milano, Italy). Cell viability was evaluated via MTT assays, and the HUVEC and HeLa (ATCC CCL-2) cell line were purchased from PromoCell (Heidelberg, Germany) and from LGC Standards S.r.l. (Milan, Italy), respectively.

^{1}H, and ^{19}F NMR spectra were recorded on 400 MHz spectrometers. Chemical shifts are expressed in ppm (δ), using tetramethylsilane (TMS) as the internal standard for ^{1}H nucleus (δH = 0.00), while C_6F_6 was used as the external standard (δF = −162.90) for ^{19}F.

Ultrapure filtrated mQ water was used to prepare the solution for the kinetic experiments of cleavage of HPNP and potentiometric titrations. HPNP was prepared according to the same procedure reported in the literature.[38] The other chemicals used both in the kinetics and in potentiometric measurements were used without any further purification.]

Functionalization of PAMAM and PEI polymers: synthesis of conjugates 1–4. General procedure: To a solution of the Michael acceptor **6** (n*1.0 equiv., where n = number of the outer primary amines of PAMAM G2, PAMAM G4, and bPEI 600 Da or secondary amines of lPEI 2 kDa) in MeOH (0.5 mL), a solution of the polymer (10 mg) in MeOH (0.5 mL) was added dropwise, and the resulting solution was stirred overnight at room temperature. The solvent was evaporated, the crude was dissolved in a HCl [4 N] in dioxane/TIPS (92.5:7.5) mixture, and the solution was stirred at rt for 6 hours. The conjugates were precipitated in diethyl ether and purified via dialysis with a SpectraPor RC membrane (MWCO = 1 kDa or 600 Da) against deionized water for 2 days. The products were lyophilized, obtaining fluorinated conjugates **1**–**4** as fluffy white solids.

Titrations: Acid-base potentiometric titrations were carried out in water at 0.3–0.5 mM concentration range. All the investigated materials were titrated in their fully protonated form. The solutions were added with a titrating solution of Me_4NOH in the range of 50-100 mM. The exact concentration of these standard solutions was determined with HCl 1.00 N Normex solution. The titration additions were carried out through manual addition with a Hamilton precision syringe. The pH was measured with a VioLab Bench pH Meter (Securlab srl) – 201 T DHS electrode. The elaborations of the titration plots were carried out with Matlab ver R2024b.

Kinetic Measurements: The cleavage of the RNA model substrate HPNP (0.2 mM concentration) was followed with a Shimadzu UV-2450 Spectrophotometer. The monitoring of the reaction course was carried out through the liberation in solution of *p*-nitrophenol that shows an intense band at λ = 400 nm. The reaction mixture was buffered at the indicated pH with phosphate buffer through the addition of NaOH. The concentrations of the catalysts are indicated in Table 3. A 10 mM concentration of tetramethylammonium perchlorate (TMAP) was added to the mixture in order to buffer the ionic strength. Warning! The perchlorate salts are potentially explosive, and consequently TMAP must be handled with care. No accidents occurred during the execution of the experiments described in this work. The k_{obs} values reported in Table 3 and Figure 3 were calculated with the initial rate method via the following formula: v_o/[HPNP]$_{initial}$, where v_o is the slope of the plot concentration versus time. The primary kinetic data are reported in the Supporting Information (see Figure S1a-j). The least-squares linear fitting procedures were carried out with software Matlab R2024b. Kinetic measurements of HPNP cleavage in serum (see Table S1) were carried out as described above, except that the medium was replaced with research-grade bovine serum (Aldrich, F0804) diluted 1:1 (v/v) with ultrapure Milli-Q water.

DLS Analysis: Via dynamic light scattering (DLS), both particle size distribution and ζ-potential were assessed. The analysis was performed on a Zetasizer Nano ZS (Malvern Instruments), comparing polymers obtained before and after complexation with the gene cargo. The analysis was performed in backscattering (173°) on samples prepared at the same concentrations as they were for transfections. The considered concentrations were reached exploiting 20 µL of 10 mg/mL aqueous polymer suspension added to 5 µL of water (nonviral vectors aqueous suspension) and 4 µL of 1 µg/µL DNA mixed with 1 µL of 100 mM NaOAc (gene suspension) separately prepared. A fraction of the polymer solution was mixed with 5 µL of the aqueous phase containing the genetic material, and the polyplex suspension was left to complex for about 10 minutes at room temperature. Following a proper dilution in PBS to reach 0.6 µg DNA dose, the polyplex suspension was prepared to a final volume of 1.6 mL for a reliable analysis.

Bio-layer interferometry: An Octet R1 system (Sartorius AG, Göttingen, Germany) was employed to detect interactions between **2**@PAMAM G4 and mRNA using streptavidin biosensors (SA). For setting tests, mRNAfluc (Promega) was adopted, then the same mRNAgfp used for in vitro assays (TriLink Biotechnologies) was used for comparative studies between functionalized and undecorated polymer. The polymer was biotinylated with NHS-PEG_4-biotin (Merck) at different molar ratios, corresponding to either one biotin per free amine (Protocol A) or one biotin per complex (Protocol B). Briefly, the polymer was diluted to 1 mg/mL in DI water, then the biotinylating agent was added and incubated for 30 minutes at room temperature. The product was purified by ultrafiltration three times using Amicon filters with a 3 kDa cutoff (Merck). BLI measurements were conducted according to the manufacturer's instructions. SA sensors were pretreated with PBS for at least 10 minutes before each measurement. Each assay consisted of a 30-second initial baseline in a tube containing PBS, a 120-second loading step in a 4 µL drop, followed by a further 30-second baseline in PBS. This was followed by a 120-second association step in a 4 µL drop containing the sample and a 120-second dissociation step in PBS. Measurements were recorded at a room temperature of 24 °C. Association and dissociation parameters were calculated using Octet N1 software (Sartorius). Curves were generated using GraphPad PRISM 6 from the recorded raw data.

Agarose Gel Analysis: Agarose gel analysis of plasmid complexes with cationic fluorinated polymers at different N/P ratios (5, 15, and 30) was performed following the complexation instructions of the transfection protocol. A total of 250 ng of pGFP (Promega) was used to form complexes with an appropriate dilution of the dendrimer in deionized water. The complexes were then diluted to a final volume of 20 µL, and 4 µL of loading dye (blue/orange loading dye 6x, Promega) was added. A total of 24 µL of each sample was loaded onto a 0.8% (w/v) agarose gel, which already contained the GREEN STAIN 10000X tool (CYANAGEN, Bologna, Italy) according to the manufacturer's instructions. A DNA ladder (BenchTop 1 kb DNA Ladder, Promega) was loaded in the first lane, while free DNA was loaded

in the last lane of the first gel. Electrophoresis was performed in Tris-acetate-EDTA buffer (1x TAE) at 70 V for 60 minutes. The gel was analyzed under a UV transilluminator (BIO-RAD ChemiDoc XRS+) using an appropriate filter.

Transfection and viability protocols: Green fluorescent protein plasmid (monsterGFP plasmid from Promega) and mRNA (EGFP CleanCap from Trilink Biotechnologies), HeLa and HUVECs were used for TE and cytotoxicity evaluation for mRNA cleavage in vitro preliminary studies and all fluorinated conjugates TE investigation, respectively. The transfection protocol involves the preparation of two separate solutions: 20 µL of 10 mg/mL of aqueous polymer suspension plus 5 µL of water and 4 µL of 1 µg/µL genetic material mixed with 1 µL of 100 mM NaOAc. A portion of polymeric suspension was mixed into 5 µL aqueous phase containing the genetic material at a concentration calibrated to establish the desired N/P ratio, and the mixture was left to complex for about 10 minutes at room temperature. Then, following a proper dilution in PBS and then in culture medium (Endothelial Cell Growth Medium MV from PromoCell for HUVEC and complete DMEM prepared with 10%FBS, 1% of Sodium Pyruvate solution 100 mM, 1% of L-Glutamine solution 200 mM, and 1% of Penicillin-Streptomycin) for HeLa to reach a 0.6 µg DNA dose or 50 ng mRNA dose, 150 µL of medium/dendriplexes was added per well for 15,000 cells per well in a 96-well plate. For cytotoxicity tests without plasmid cargo, the dendrimer suspension was mixed with 5 µL of PBS. Cell viability was evaluated via MTT assay, performed by replacing the culture medium with the same amount of 1x MTT + PBS/culture medium solution and incubating the cells for 4 hours. After incubation, DMSO was added to dilute the MTT-formazan formed by metabolically active cells, and spectrophotometric measurement via TECAN SPARK Multimode Microplate Reader of MTT-formazan at 570 nm was performed to quantify cell viability.

Image analysis for GFP fluorescence and percentage of transfected cells: For TE studies, GFP fluorescence intensity measure and the percentage of transfected cells was evaluated with ImageJ.[39,40] The cell counting has been settled with the software analyzing each image with specific tools, Brightness & Contrast, the Thresholding method, and Find Edges, to perform the cell count implemented with the Analyze Particle tool. The final percentage of transfected cells was obtained considering the ratio between the number of transfected cells and the total number of cells of the images acquired with CELENA S with the GFP filter cube and in brightfield mode, respectively. The GFP fluorescence was evaluated as corrected total cell fluorescence (CTCF).

Statistical analysis: Data are presented as mean ± standard deviation (SD) from four independent replicates ($n = 4$). For all experiments conducted in quadruplicate, almost 10 images for each replicate were acquired with CELENA S using a PlanAchro 4x objective lens without a prolongate light microscope exposure of culture cells. Student's t-test was used to determine statistical significance, considering $p < 0.05$ as significant using OriginLab-OriginPro (Northampton, MA, USA).

Supporting Information

Supporting Information is available from the Wiley Online Library or from the author.

Acknowledgments

Politecnico di Milano and CNR are gratefully acknowledged for economic support. The authors wish to express warm gratitude to Miss Martina Lucrezia Chiaveri, Miss Valentina Milone, Mr. Matteo Ratti and Mr Davide Savore for helping in the experimental work.

Open access publishing facilitated by Politecnico di Milano, as part of the Wiley - CRUI-CARE agreement.

Conflicts of Interest

The authors declare no conflicts of interest.

Data Availability Statement

The data that support the findings of this study are available in the supplementary material of this article

Keywords: antisense therapy · artificial ribonucleases · dendrimers · enzyme mimics · fluorine · transfection efficiency

[1] Z. J. Leśnikowski, *ChemMedChem* **2025**, *20*, e202400493.
[2] S. Gadde, *Med. Chem. Commun.* **2015**, *6*, 1916.
[3] R. G. Gish, P. M. Gholam, *Clevel. Clin. J. Med.* **2009**, *76*, S20.
[4] M. C. Bellucci, C. Romani, M. Sani, A. Volonterio, *Antibiotics* **2024**, *13*, 783.
[5] X. Sun, S. Setrerrahmane, C. Li, J. Hu, H. Xu, *Sig Transduct Target Ther* **2024**, *9*, 316.
[6] M. Catani, C. De Luca, J. Medeiros Garcia Alcantara, N. Manfredini, D. Perrone, E. Marchesi, R. Weldon, T. Muller-Spath, A. Cavazzini, M. Morbidelli, M. Sponchioni, *Biotechnol. J.* **2020**, *15*, e1900226.
[7] K. Sridharan, N. J. Gogtay, *Br. J. Clin. Pharmacol.* **2016**, *82*, 659.
[8] X. Bian, L. Zhou, Z. Luo, G. Liu, Z. Hang, H. Li, F. Li, Y. Wen, *ACS Nano* **2025**, *19*, 4039.
[9] N. Bono, F. Ponti, D. Mantovani, G. Candiani, *Pharmaceutics* **2020**, *12*, 183.
[10] H. Zu, D. Gao, *AAPS J.* **2021**, *23*, 78.
[11] Y. Xu, J. Chen, J. Ding, J. Sun, W. Song, Z. Tang, C. Xiao, X. Chen, *Polym. Sci. Technol.* **2025**, *1*, 171.
[12] C. Dufes, I. F. Uchegbu, A. G. Schatzlein, *Adv. Drug Delivery Rev.* **2005**, *57*, 2177.
[13] G. Navarro, C. Tros de Ilarduya, *Nanomedicine* **2009**, *5*, 287.
[14] S. L. Mekuria, J. Li, C. Song, Y. Gao, Z. Ouyang, M. Shen, X. Shi, *ACS Appl. Bio Mater.* **2021**, *4*, 7168.
[15] I. Tirotta, V. Dichiarante, C. Pigliacelli, G. Cavallo, G. Terraneo, F. B. Bombelli, P. Metrangolo, G. Resnati, *Chem. Rev.* **2015**, *115*, 1106, https://doi.org/10.1021/cr500286d.
[16] J. Lv, Y. Cheng, *Chem. Soc. Rev.* **2021**, *50*, 5435.
[17] M. Egli, M. Manoharan, *Nucl. Acids Ther.* **2023**, *51*, 2529.
[18] K. C. Remant Bahadur, B. Thapa, J. Valencia-Serna, H. M. Aliabadi, H. Uludağ, *J Control. Release* **2017**, *256*, 153.
[19] M. N. Zhao, R. J. Wang, K. M. Yang, Y. H. Jiang, Y. C. Peng, Y. K. Li, Z. Zhang, J. X. Ding, S. J. Shi, *Acta Pharm. Sin. B* **2023**, *13*, 916.
[20] C. Romani, P. Gagni, M. Sponchioni, A. Volonterio, *Bioconjugate Chem.* **2023**, *34*, 1084. https://doi.org/10.1021/acs.bioconjchem.3c00139.
[21] C. Romani, P. Gagni, M. E. Di Pietro, M. Sani, M. Sponchioni, A. Volonterio, *Bioconjugate Chem.* **2025**, *36*, 66.
[22] R. Salvio, A. Casnati, *J. Org. Chem.* **2017**, *82*, 10461.
[23] D. Lisi, C. A. Vezzoni, A. Casnati, F. Sansone, R. Salvio, *Chem. - Eur. J.* **2023**, *29*, e202203213.
[24] C. A. Vezzoni, A. Casnati, S. Orlanducci, F. Sansone, R. Salvio, *ChemCatChem* **2024**, *16*, e202301477.
[25] J. Kofoed, J.-L. Reymond, *Curr. Opin. Chem. Biol.* **2005**, *9*, 656.

[26] M. Molteni, M. C. Bellucci, S. Bigotti, S. Mazzini, A. Volonterio, M. Zanda, *Org. Biomol. Chem.* **2009**, *7*, 2286.
[27] C. Sgorbati, E. Lo Presti, G. Bergamaschi, M. Sani, A. Volonterio, *J. Org. Chem.* **2021**, *86*, 9225.
[28] C. Romani, M. Sponchioni, A. Volonterio, *Pharm Int* **2024**, *41*, 1725.
[29] B. Xu, M. I. Jacobs, O. Kostko, M. Ahmed, *ChemPhysChem* **2017**, *18*, 1503.
[30] A. Casnati, R. Salvio, *Coord. Chem. Rev.* **2025**, *531*, 216479.
[31] R. Salvio, M. D'Abramo, *Eur. J. Org. Chem.* **2020**, *2020*, 6004.
[32] R. Salvio, M. Moliterno, D. Caramelli, L. Pisciottani, A. Antenucci, M. D'Amico, M. Bella, *Catal. Sci. Technol.* **2016**, *6*, 2280.
[33] R. Salvio, S. Volpi, R. Cacciapaglia, F. Sansone, L. Mandolini, A. Casnati, *J. Org. Chem.* **2016**, *81*, 9012.
[34] A. Jug, T. Bratkovič, J. Ilaš, *Trends Anal. Chem.* **2024**, *176*, 117741.
[35] J. Casper, S. H. Schenk, E. Parhizkar, P. Detampel, A. Dehshahri, J. Huwyler*J. Controlled Release* **2023**, *362*, 667.
[36] M. Khan, C. Y. Ang, N. Wiradharma, L. K. Yong, S. Q. Liu, L. H. Liu, S. J. Gao, Y. Y. Yang, *Biomaterials* **2012**, *33*, 4673.
[37] A. Bielinska, J. F. Kukowska-Latallo, J. Johnson, D. A. Tomalia, J. R. Baker Jr., *Nucleic Acid Res* **1996**, *24*, 2176.
[38] D. M. Brown, D. A. Usher, *J. Chem. Soc.* **1965**, 6558, https://doi.org/10.1039/JR9650006558.
[39] C. A. Schneider, W. S. Rasband, K. W. Eliceiri, *Nat. Methods* **2012**, *9*, 671.
[40] C. T. Rueden, J. Schindelin, M. C. Hiner, B. E. DeZonia, A. E. Walter, E. T. Arena, K. W. Eliceiri, *BMC Bioinformatics* **2017**, *18*, 529.

Manuscript received: June 27, 2025
Revised manuscript received: October 27, 2025
Version of record online: ■■, ■■